The Supporting Information (SI) for "Optical Sensors for In-Situ Real-Time Detection of Ammonia"

Some experimental details and the experimental data mentioned in the main text are as follows:

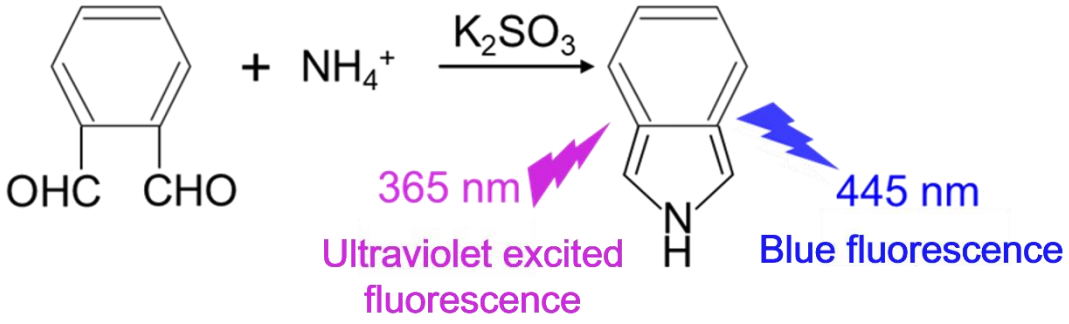

Figure S1. Fluorescence Luminescence Principle

In this experiment, potassium sulfite (K_2SO_3) and o-phthalaldehyde (OPA) are mixed under alkaline conditions to facilitate a fluorescence derivatization reaction with ammonia (NH_3) or ammonium ions (NH_4^+). The mechanism involves sulfite ions (SO_3^{2-}) activating the aldehyde group of OPA, enabling OPA to react with ammonia and form a highly fluorescent isoindole derivative. This derivative exhibits strong fluorescence at 340/425 nm (excitation/emission), with intensity proportional to ammonia concentration. The reaction demonstrates high selectivity (minimal interference from amino acids or metal ions), exceptional sensitivity, and rapid kinetics, making it suitable for trace ammonia detection.

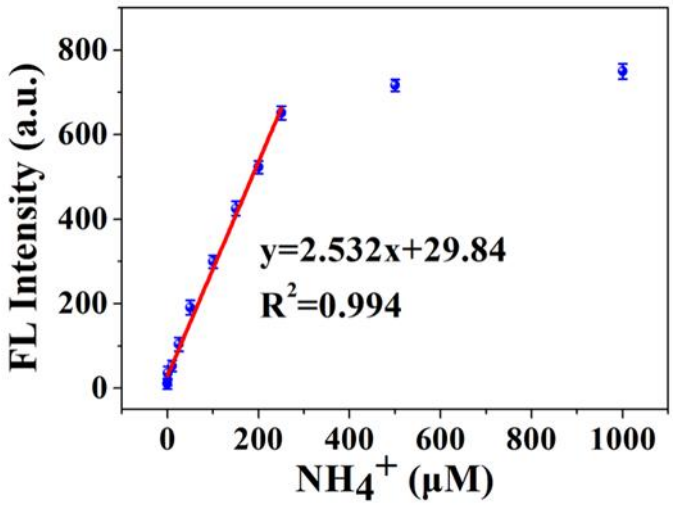

Figure S2. Linear Range of the Fluorescence Detection System

Based on preliminary experiments conducted under the operational parameters of this fluorescence detection system, the fluorescence intensity exhibits a strong linear correlation ($R^2 \geq 0.994$) with ammonia concentration across the range of 0–280 μM.

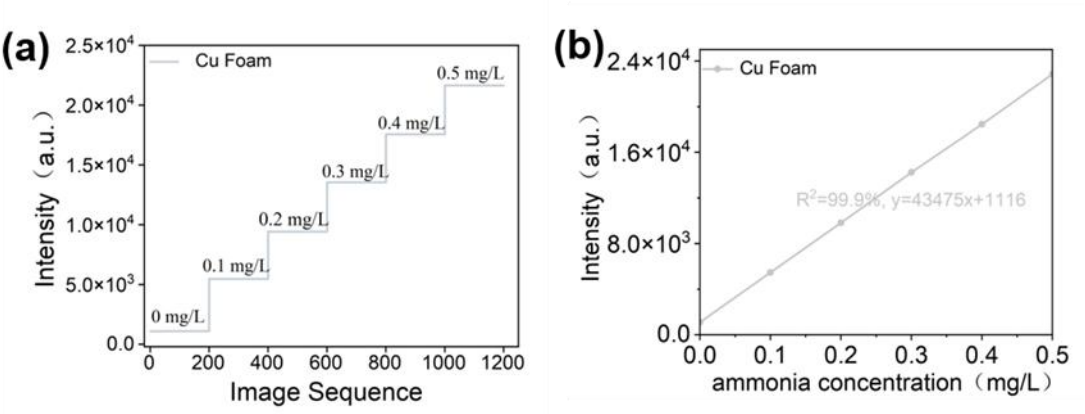

Figure S3. Calibration Steps and Fitted Line for Copper Foam Electrode

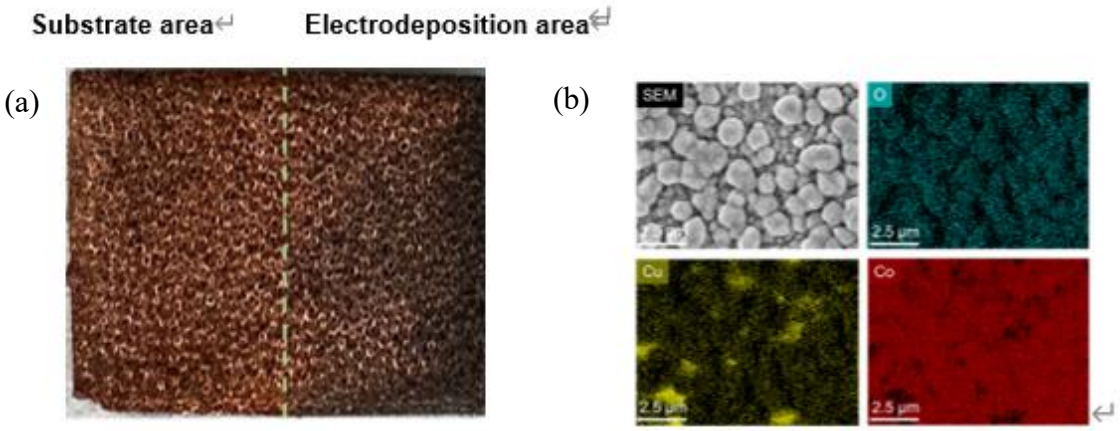

Figure S4. Metal Specimen of Foam Copper with Asymmetrically Deposited Cobalt and Its Elemental Distribution

Figure 4 depicts the foam copper metal specimen with asymmetrically deposited Co (as described previously). EDS analysis was conducted on the right-side Co-electrodeposited region of the sample. The corresponding microstructural features and elemental distribution maps for oxygen (O), copper (Cu), and cobalt (Co) are displayed in the right panel.Figure S4(a) shows the photograph of the half‑ deposited electrode, and Figure S4(b) presents the elemental distribution from EDS characterization of the copper foam substrate and the electrodeposited cobalt.

Figure 5 depicts the surface modification of multiple foam metal catalysts via electrodeposition, showing comparative images of the catalysts pre- and post-modification alongside their corresponding elemental distribution maps.

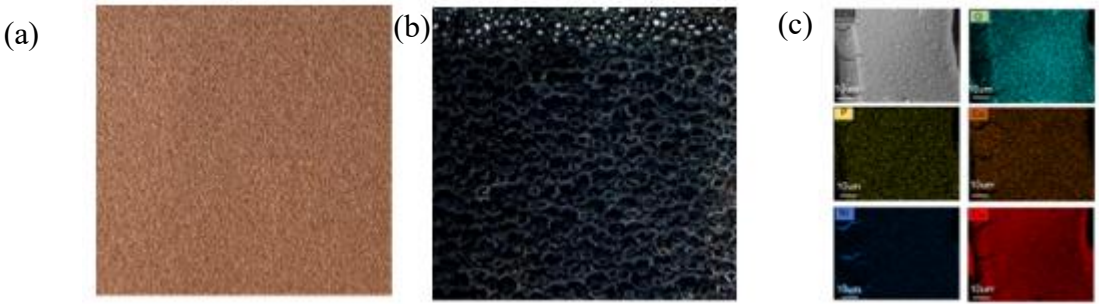

Figure S5. Comparative Elemental Distribution in Foam Metal Substrates and Modified Specimens

Figure S5(a) shows the photograph of pristine copper foam, Figure S5(b) shows the photograph of copper foam after electrodeposition in the prepared electrolyte, and Figure S5(c) presents the elemental distribution characterized by EDS after electrodeposition.Similarly, Figure S5(d) shows the photograph of pristine Fe–Ni foam, Figure S5(e) shows the photograph of Fe–Ni foam after electrodeposition in the prepared electrolyte, and Figure S5(f) presents the elemental distribution characterized by EDS after electrodeposition.

Figures S6 and S7 display the results of fluorescence measurements for several metal catalysts in standard ammonia solutions of varying concentrations. Figure 6 presents the raw fluorescence images, while Figure 7 shows the processed calibration steps and fitted linear regression line.

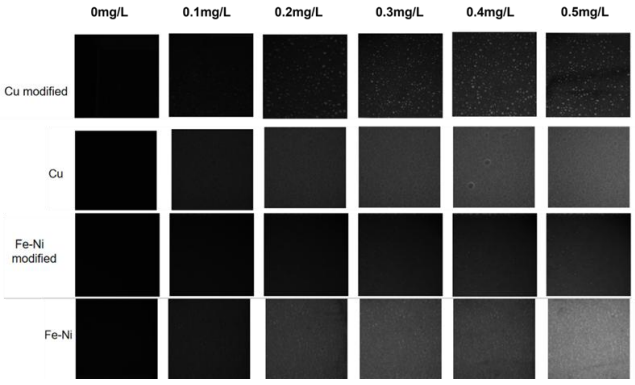

Figure S6. Raw Data Plots of Calibration for Several Foam Metals

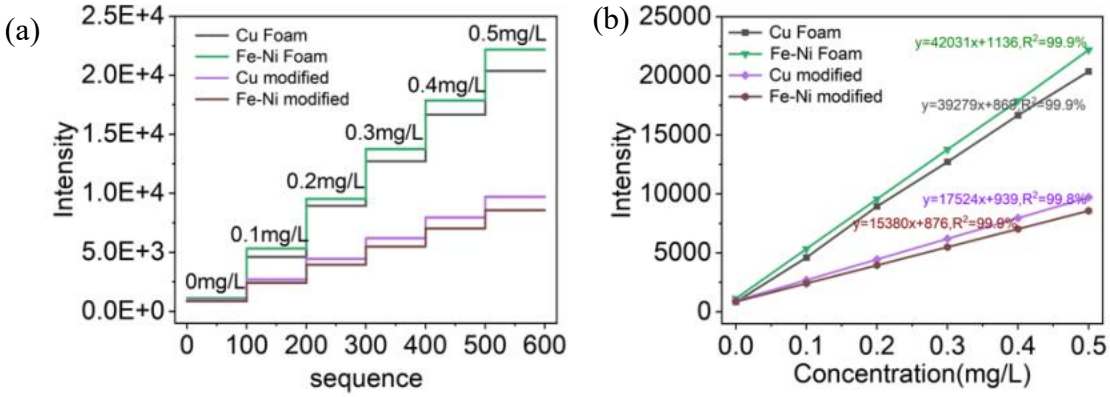

Figure S7. Calibration Steps and Linear Fitting Lines for Several Foam Metals

Figure 6 shows the imaging photographs of the four catalysts in ammonia solutions with

corresponding concentrations. Figure 7(a) presents the calibration steps of the four catalysts, and Figure 7(b) shows the corresponding fitting curves.

The experiment on the crystallinity of the iron-nickel alloy and its corresponding electrodeposition-modified catalyst， XRD experiments have been supplemented to measure the crystallinity under the corresponding electrodeposition conditions, and the specific experimental results are shown in the following figure:

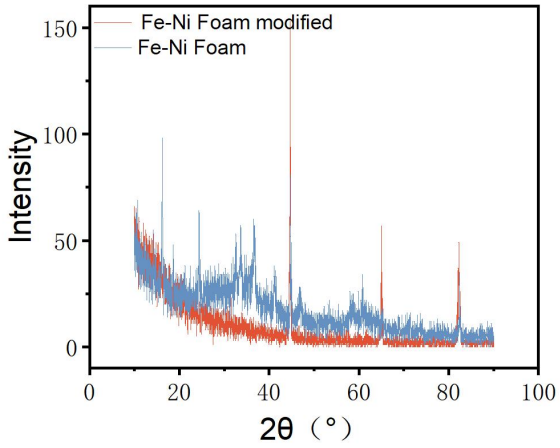

Figure S8. Experimental results of crystallinity characterized by XRD

The crystallinity was calculated according to the following formula:

$$X_c = A_c / (A_c + A_a)$$

Where Xc represents the crystallinity, Ac is the total integrated area of crystalline diffraction peaks, and Aa is the total integrated area of the amorphous scattering halo.

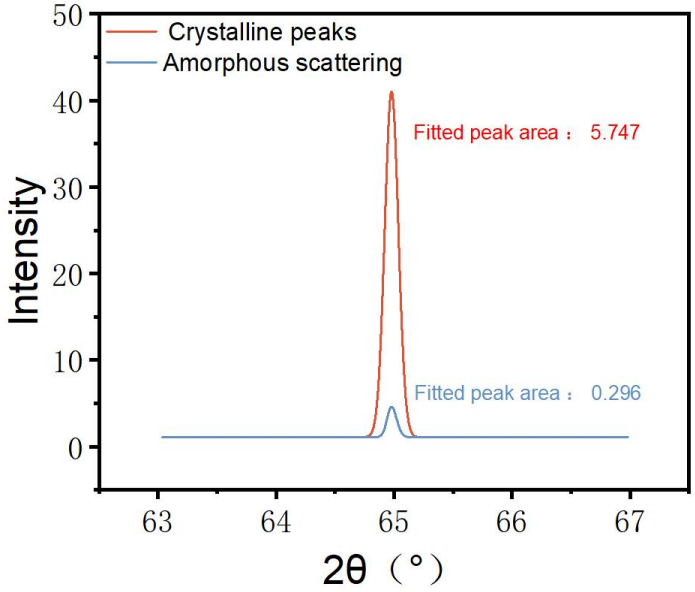

Figure S9. The detailed calculation process of crystallinity

After background subtraction and peak-fitting processing of the XRD pattern, the total area of all crystalline diffraction peaks Ac and the total area of the amorphous scattering peak Aa were integrated separately. As an example, the calculation for one peak is presented as Figure R2:

$$X_c=A_c/(A_c+A_a)=5.747/(5.747+0.296)=0.951$$

The total areas of all crystalline diffraction peaks and amorphous scattering peaks were calculated as 40.147 and 2.633, respectively. Substituting these values into the formula yields the overall crystallinity:

$$40.147/(40.147+2.633)=0.938$$

In this section, the fluorescence reaction mechanism has been further supplemented:

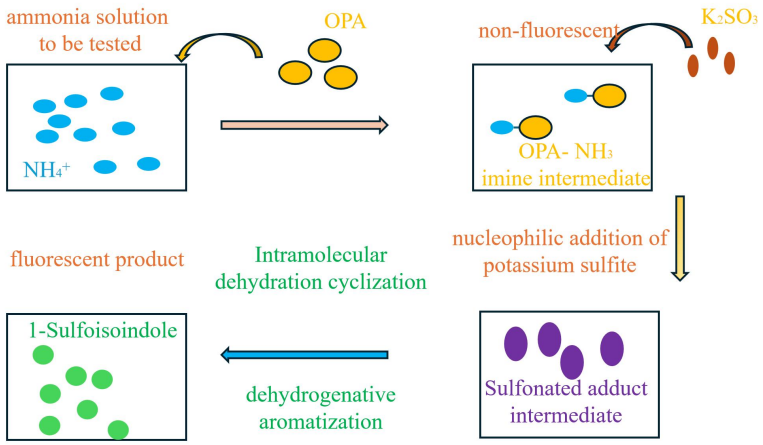

Figure S10. Fluorescence reaction mechanism

Under weakly alkaline conditions, the species dissociated from potassium sulfite react with o-phthalaldehyde (OPA) to form water-soluble intermediates and activate the aldehyde groups. Ammonia in the system acts as a nucleophile and undergoes nucleophilic addition and dehydration condensation with the intermediates, followed by intramolecular cyclization to produce isoindole derivatives with strong fluorescence properties. The reaction kinetics are fast, and the fluorescence intensity is quantitatively positively correlated with ammonia concentration, enabling highly sensitive fluorescence detection of ammonia nitrogen. The above mechanistic explanations have been added to the corresponding mechanism discussion in the Supporting Information.

This study has systematically completed the testing and characterization of key performances such as detection accuracy and repeatability of the sensor, and improved the relevant data description in the main text.

For accuracy, calibration experiments were carried out in the ammonia concentration range of 0–0.6 mg/L. The correlation coefficient of the fitted straight line is R^2 = 0.99973, and the system standard deviation, sensitivity and concentration resolution were also determined to quantitatively characterize the detection accuracy of the sensor.

Furthermore, standard ammonia solutions with prepared concentrations of 0.15 mg/L, 0.25 mg/L and 0.35 mg/L were tested in the system. The test results are shown in the following figure, and R^2 = 0.995 for the linear fitting with the calibration line, indicating good accuracy of the test results.

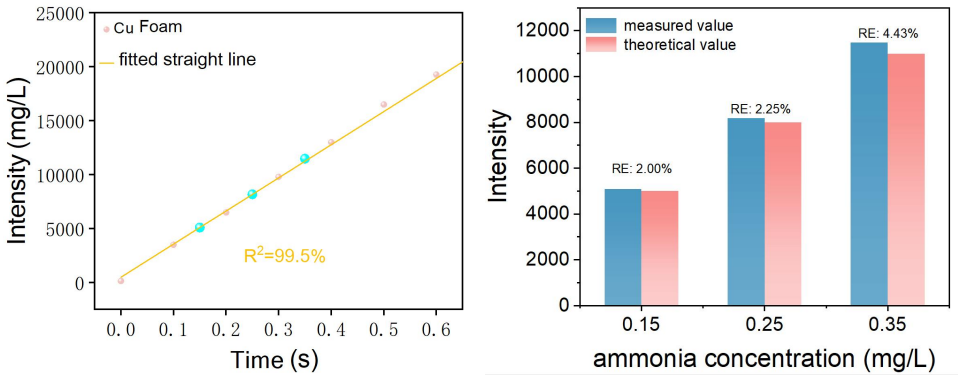

Figure S11. Accuracy of the system test

To verify the stability and repeatability of the system, a standard ammonia solution with a concentration of 0.15 mg/L was selected in this experiment. Three repeated calibration experiments were performed in the system using foam copper as the working electrode. A comparative analysis of the experimental results shows that the data fluctuation of the three calibration results is less than 5%, indicating that the experiment exhibits favorable repeatability and stability.

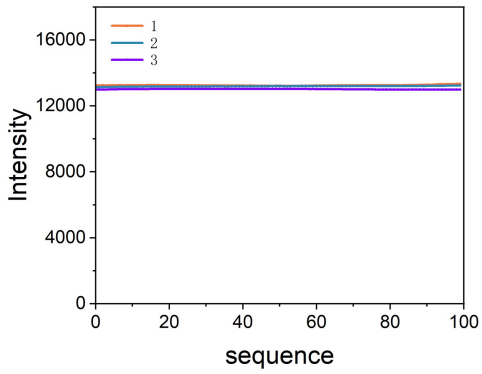

Figure S12. Stability and repeatability tests

The results show that the fluorescent reagent has no significant influence on the electroreduction reaction, ensuring the stability of the detection system.

For repeatability, three parallel electroreduction detection experiments were carried out on the electrolyte containing fluorescent reagent, and the experimental results showed good consistency, confirming that the sensor has excellent detection repeatability.

This study has supplemented the selectivity investigation of the sensor, and systematically explored the effects of solution pH and common coexisting ions on the detection results.

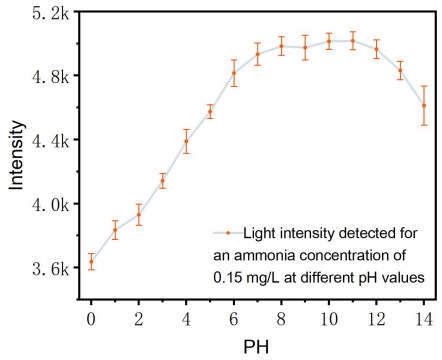

Figure S13. pH applicable range

Regarding the influence of pH value, the acidity and alkalinity of the solution were adjusted by sulfuric acid and sodium hydroxide to determine the pH applicable range of the fluorescent reagent. The experimental results show that the fluorescence response of this detection system is stable in the pH range of 7–10, with no significant

deviation in the detection results, which is consistent with the applicable range reported in relevant literature.

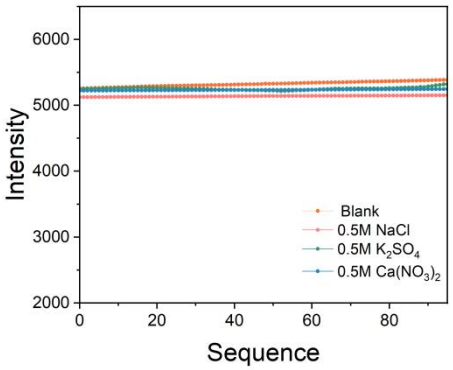

Figure S14. Interference ion coexistence test

For the coexisting ion interference test, common coexisting ions in the electrocatalytic nitrate reduction system were added into the detection system. Using a blank group as the control, calibration comparison experiments were carried out by adding 0.5 M NaCl, 0.5 M K_2SO_4, and 0.5 M $Ca(NO_3)_2$ to introduce Na^+ and Cl^-, K^+ and SO_4^{2-}, and Ca^{2+} and NO_3^-, respectively. The results are shown in the following figure, indicating that these common coexisting ions have no obvious influence on the response of the fluorescent reagent, and the sensor exhibits excellent detection selectivity toward ammonia/ammonium ions.

This study has supplemented the research on the linear response range of the copper-based working electrode to ammonia and verified the sensor's detection performance for ammonia concentrations higher than 0.6 mg/L. The experimental results show that in the ammonia concentration range of 0–0.6 mg/L, the fluorescence intensity of the copper-based electrode has a good quantitative positive correlation with the ammonia concentration, with excellent fitting correlation, which meets the requirements of quantitative detection. However, in the calibration experiment in the concentration range of 0 – 0.7 mg/L, the linear response accuracy of the system decreases to 99.2%, and the experimental quantitative detection error in the figure increases.To better illustrate the calibration error, a bar chart comparing the

theoretical and measured values at 0.7 mg/L was provided in this study. It can be seen that the measurement accuracy is higher in the range of 0–0.6 mg/L.

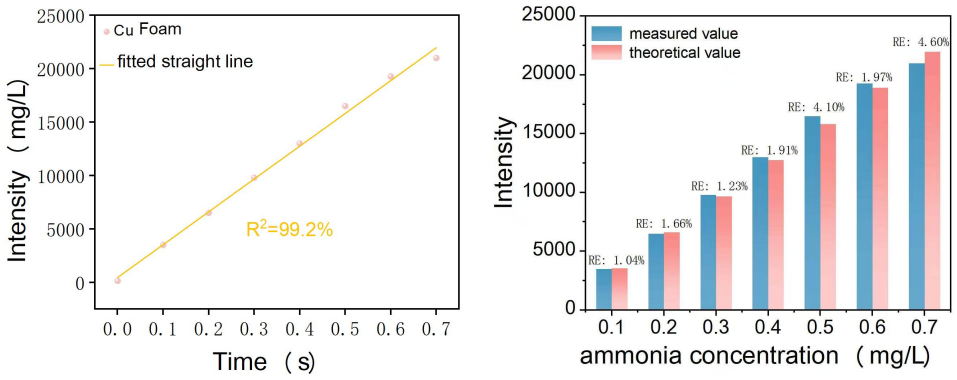

Figure S15. Concentration-intensity linear fitting plot

To ensure the experimental detection accuracy and achieve accurate comparison and quantitative analysis of ammonia production at different spatial positions of the catalyst, the effective linear detection range of the sensor for ammonia was determined to be 0–0.6 mg/L in this study. The sensor cannot achieve accurate quantitative detection above this concentration. Therefore, all relevant experiments in this study were carried out within the linear detection range of 0–0.6 mg/L.

The specific calculation process is as follows: In this study, the full width at half maximum (FWHM) is used to quantify the spatial uniformity of ammonia concentration on the electrode surface. Its definition and calculation procedure are: first, the "maximum frequency of concentration occurrence" is extracted from the frequency histogram of ammonia concentration distribution, and half of this value is taken as the "half-peak frequency"; then, the two corresponding concentration values at which the ordinate of the histogram equals the half-peak frequency (the left low-concentration boundary and the right high-concentration boundary) are determined, and the difference between them is defined as FWHM. In this paper, the FWHM values are 0.0027 at 60 s and 0.0072 at 195 s, reflecting the dynamic change in the spatial uniformity of ammonia concentration distribution with the reaction process — the smaller the FWHM value, the smaller the difference in ammonia concentration between different regions on the electrode surface at the same moment, and the more uniform the catalytic activity. On this basis, the FWHM of the ammonia concentration distribution peak in Figure 3(c) has been calculated, and the specific values have been added and labeled in Figure 3(c) of the main text. The FWHM values corresponding to different reaction times are as follows: 60 s (0), 105 s (0.0027), 150 s (0.0041), 195 s (0.0072). These values intuitively reflect the change in the spatial uniformity of ammonia concentration on the electrode surface during the electroreduction process, providing a quantitative basis for the analysis of spatial heterogeneity in the catalytic reaction.

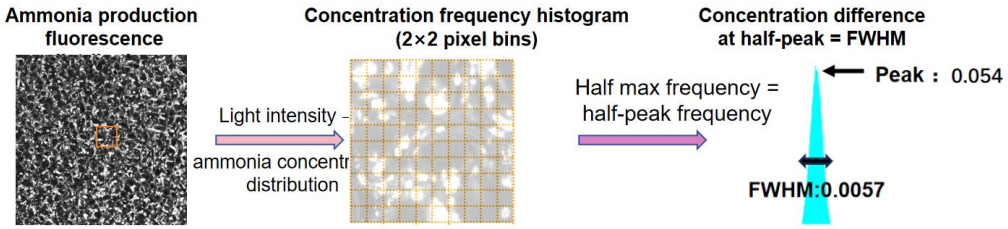

Figure S16. Calculation Process of FWHM